

Recent Progress of Additive Manufactured Ti-6Al-4V by Electron Beam

Melting

Pan Wang^{1*}, Mui Ling Sharon Nai^{1**}, Xipeng Tan², Guglielmo Vastola³, Srinivasan Raghavan¹, Wai Jack Sin¹, Shu Beng Tor², Qing Xiang Pei³, Jun Wei¹

¹Singapore Institute of Manufacturing Technology, 73 Nanyang Drive, 637662, Singapore

²Singapore Centre for 3D Printing, School of Mechanical & Aerospace Engineering, Nanyang Technological University, 50 Nanyang Avenue, 639798 Singapore

³Institute of High Performance Computing, 1 Fusionopolis Way #16-16, Connexis, Singapore 138632

Corresponding authors: *Email: wangp@simtech.a-star.edu.sg, Phone: +65 6793 8957

**Email: mlnai@simtech.a-star.edu.sg, Phone: +65 6793 8976

Abstract

Electron beam melting (EBM) is one of the powder-bed fusion additive manufacturing technologies. This technology is very suitable for producing near-net-shape small to medium volume metallic parts with complex geometries. However, layer-by-layer fusion step introduces rapid thermal cycles, which results in a different microstructure as compared to their cast or wrought counterparts. Therefore, the microstructure and mechanical properties produced by EBM must be better understood and in turn to control the microstructure for requirements of some specific applications. Accordingly, in this paper, an insight will be provided on the effort of understanding the microstructure and mechanical properties from atomic scale to real complex big-sized industrial components. The spatial- and geometrical-based microstructure and mechanical properties of EBM Ti-6Al-4V as well as the effect of heat treatment on them were investigated using atom probe tomography, transmission electron microscopy, scanning electron microscopy, optical microscopy, x-ray diffraction, x-ray computed tomography, nanohardness testing, microhardness testing, tensile testing and finite element simulations. The microstructure and deformation mode depend on both the build thickness and build height which are closely linked to the heat input and the cooling rate in EBM process. Furthermore, the control of microstructure by varying the process parameters and heat treatment schemes was also proposed. By using these findings, an impeller prototype with a base diameter of 100 mm, a height of 53 mm and thinnest sections of ~0.7 mm and a turbine blade prototype with dimensions of 180×70×360 mm were successfully fabricated by EBM. These components exhibited an overall improved combination of strength and ductility as compared to the counterparts fabricated by conventional methods. These results revealed that EBM is a promising method for fabricating complex-shaped industrial components with superior mechanical performance for practical application.

Keywords: 3D printing; titanium alloy; microstructure; mechanical properties; phase transformation, porosity, surface finishing, residual stress, simulation

Introduction

Additive manufacturing (AM), also known as rapid prototyping, three-dimensional printing or solid freeform fabrication, has become an emerging technology in the manufacturing industry, enabling the production of functional components directly from computer aided design models [1, 2]. Electron Beam Melting (EBM) is one of the powder-bed fusion (PBF) AM techniques for near-net-shape manufacture of high value added and small to medium volume components [3, 4]. In an EBM system, high energy density electron beam was generated to selectively melt the powder bed and it is theoretically able to process any metallic materials with high melting points under elevated temperatures and high vacuum atmosphere. The high vacuum atmosphere is suitable for reactive metallic materials, such as Ti alloys. Among all of these Ti alloys, Ti-6Al-4V, which has extensive applications in biomedical and aerospace fields in the past few years [5-7], is the most developed material for EBM processing [4, 8, 9]. The microstructure and mechanical properties of EBM-built Ti-6Al-4V parts have been extensively investigated in the past few years. The mechanical properties of EBM-built small parts with simple geometries were revealed to be comparable with wrought counterparts [10]. It is, however, not sufficient in the view of both academic interest and industrial applications. For academic interest, it is still lacking the quantitative studies to reveal the microstructure evolution during EBM processing to further guide the development of new materials. Furthermore, in order to realize direct fabrication of industrial components using EBM, it is necessary to not only understand the influence of build height, build thickness and build geometry on component's resultant microstructure and properties but also to tailor the microstructures and properties to suit the requirements of specific applications. In addition, it is essential to understand and control pore size and pore distribution in EBM-built parts to ensure that the built part is a fully functional component rather than just a prototype. Therefore, the present paper is to summarize the efforts taken in Singapore Institute of Manufacturing Technology (SIMTech) and our collaborators to elucidate the above critical scientific issues. In the following sections, we will present experiments as well as simulations' findings which are tailored to deepen our experience and understanding of EBM process.

Spatial and geometrical-based microstructure and mechanical properties

We conducted systematic and quantitative characterization on microstructure and mechanical properties of EBM-built Ti-6Al-4V [4, 11-15]. Fig. 1 shows the illustration of EBM system and parts that were prepared to evaluate the effects of build thickness, build height and complex geometry on the microstructure and mechanical properties. Their dimensions are listed in Table 1. By utilizing the atom probe tomography, transmission electron microscopy, scanning electron microscopy, optical microscopy, x-ray diffraction, and finite element simulations, we revealed that the microstructure is dependent on the build thickness, build height, and build geometry [4, 13-15]. For the parts with simple geometry, a mixed microstructure of α/β and martensite plates was observed in the thin wall specimen (≤ 1 mm), while α/β dual phase microstructure was found in the other specimens [13]. With the

increase of build thickness and build height, the α/β dual phase microstructure became coarser, which was evaluated by the α lath width or β rod spacing [13-15]. In addition, a graded microstructure was observed along the build direction. For the part with complex geometry, however, the microstructure was much more complex as compared to that of a simple geometry and it is dependent on the thermal history experienced by the sections [4]. Furthermore, additions of support structures at the bottom section could change the cooling rates at both the top and bottom sections, resulting in a change in graded microstructure [4].

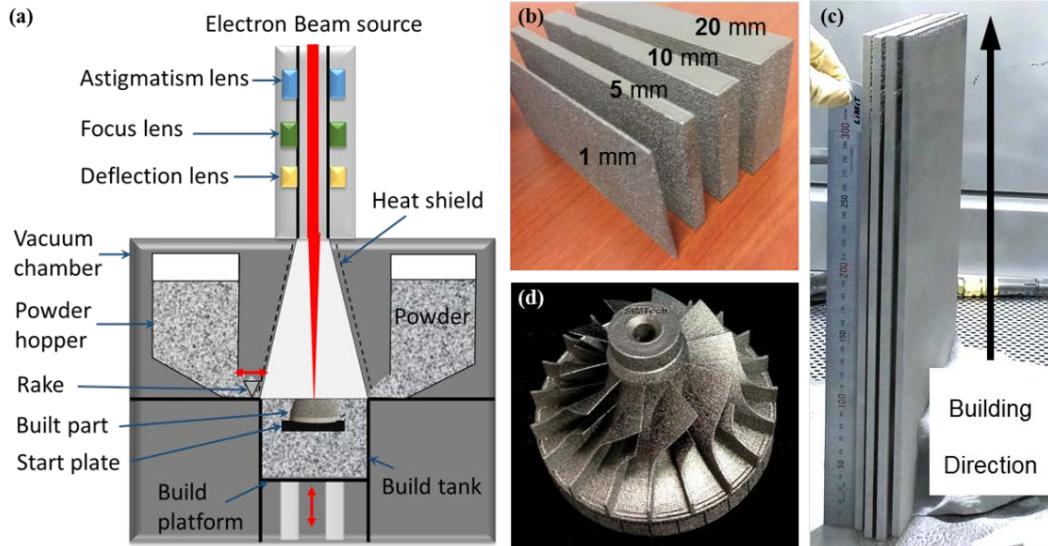


Fig. 1 (a) Illustration of EBM system and pictures of samples prepared by Arcam EBM machines to evaluate the effects of (b) build thickness, (c) build height and (d) complex geometry on the microstructure and mechanical properties of EBM-built parts.

Table 1 Dimensions of EBM-built parts and their related purpose

Specimens No.	Width (mm)	Length (mm)	Height (mm)	Purpose
1	1	100	30	Build thickness
2	5	100	30	Build thickness
3	10	100	30	Build thickness
4	20	100	30	Build thickness and build height
5	6	180	372	Build height and anisotropic mechanical properties
6	100	100	53	Complex geometry with thinnest sections of 0.7 mm and thickest sections of 45 mm

In order to confirm the phase constitutions in the microstructure of EBM-built Ti-6Al-4V samples with varying build thickness (Fig. 1b), we utilized the atom probe tomography to quantitatively analyze their chemical composition at atomic scale [12]. Fig. 2a reveals coexistence of α' martensite and α phase in the thin EBM-built Ti-6Al-4V sample (1 mm in build thickness). Some α' martensite was found to be retained due to partial thermal decomposition. By contrast, there are only α/β dual phases in the thick EBM-built Ti-6Al-4V sample (10 mm in build thickness, Fig. 2b), which is attributed to full decomposition of resultant martensite. Furthermore, we have found that martensitic microstructure would appear at the topmost region of EBM-built Ti-6Al-4V samples regardless of their build thickness [12]. Therefore, it can be concluded that martensitic transformation, including formation and decomposition, takes place during EBM processing of Ti-6Al-4V alloy under current optimized process parameters.

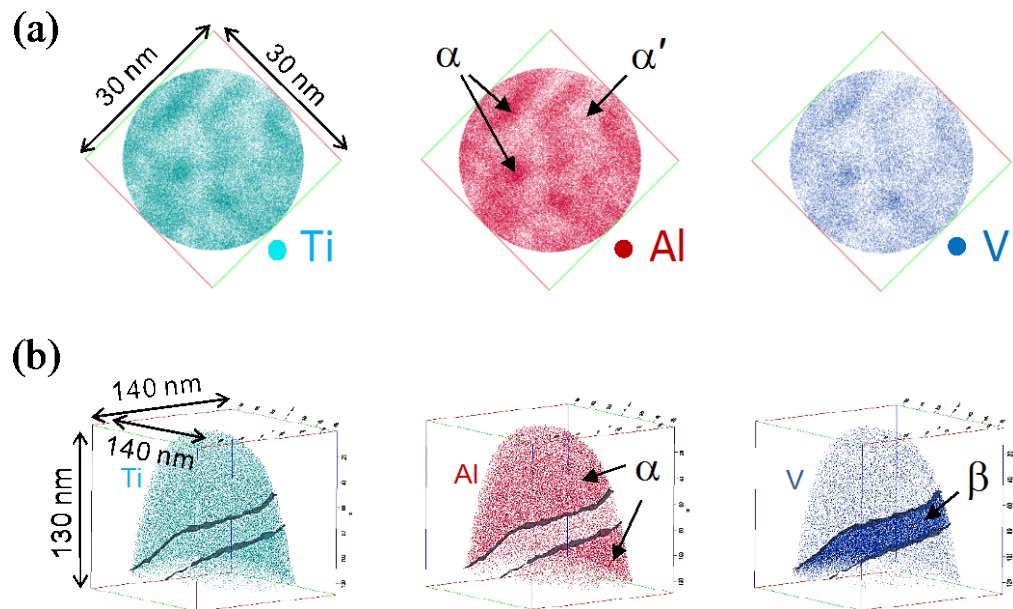
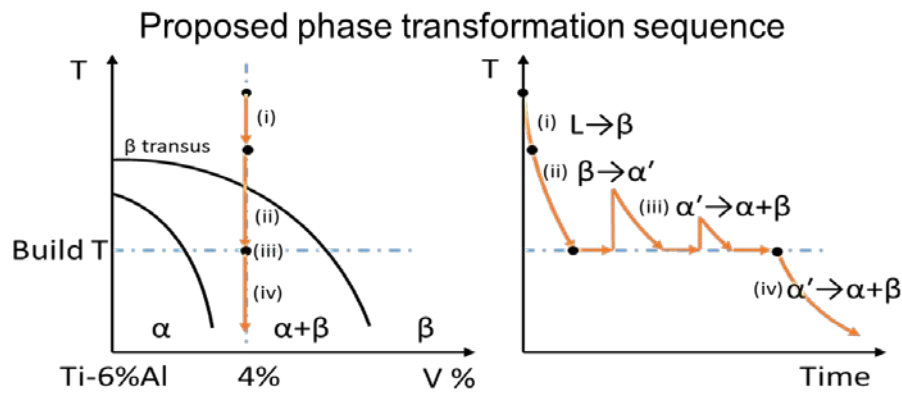


Fig. 2. Atom probe tomography analysis showing retained α' phase and fully decomposed α/β dual phases in EBM-built Ti-6Al-4V samples with build thicknesses of (a) 1 mm and (b) 10 mm, respectively.

According to the observed microstructure and the quantitative chemical composition analyses, we proposed a complete phase transformation path involved in EBM processing of Ti-6Al-4V [12, 14], as shown in Fig. 3. Wavy β grains formed from melt Ti-6Al-4V and transformed into the dominant twined α' plates with some retained β phase. This martensitic phase transformation occurred during the EBM processing, regardless of build thickness, build height and build geometry. After which, the α' plates were completely or partly transformed to α/β dual phase microstructure depending on the sections of EBM-built parts. Specifically, martensitic phase was still observed in the thin wall structure and the topmost layers of EBM-built parts [12, 13, 16].



Schematic of thermal cycling of EBM processing of Ti-6Al-4V

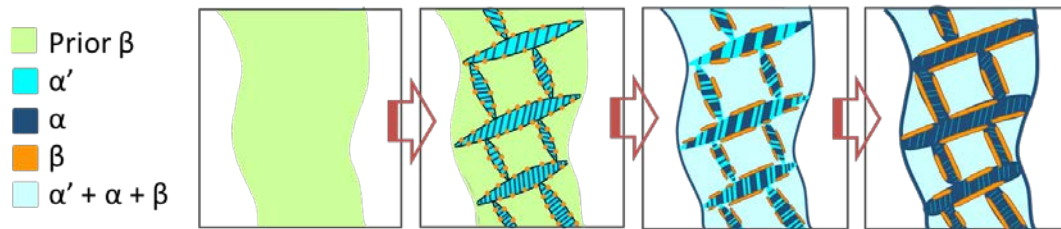


Fig. 3 Illustration of phase transformation sequence in EBM-built Ti-6Al-4V.

Besides, we also clarified the degradation of strength in EBM-built Ti-6Al-4V. For EBM-built parts with simple geometry, graded mechanical properties of Ti-6Al-4V with degraded microhardness and tensile properties were observed from bottom to top according to building height [11, 14, 15] and from thin to thick according to build thickness [4, 13]. This is in agreement with the Hall-Petch relation, indicating that the graded properties takes place mainly due to the graded microstructure. Furthermore, we also found that the α/β interface strengthening plays the primary role in determining the strength of EBM-built Ti-6Al-4V [12, 14]. The increasing α/β lattice mismatch and α/β interface width are believed to account for the strength degradation from the microscopic view [12]. Nevertheless, β grain refinement strengthening seems to be more effective as the prior β grain boundaries could absorb a higher amount of dislocations in comparison with the α/β interfaces [14].

Although the graded strength was observed in EBM-built parts, the minimum strength value of the parts was still comparable with that of wrought materials. This indicated that these EBM-built components exhibited an overall improved combination of strength and ductility as compared to the counterparts fabricated by conventional methods. These results revealed that EBM is a promising method for fabricating complex-shaped industrial components with superior mechanical performance for practical application.

Microstructure control by modifying processing parameters and post heat treatment

There are two methods to control the microstructure, firstly by varying the processing parameters and secondly by conducting post heat treatment, which in turn allows tailoring of the mechanical properties for specific applications. By varying five main processing parameters (speed function, line offset, focus offset, reference length and average currents), it is possible to modify the resultant microstructure and mechanical properties. Fig. 4 shows the picture of one of the 6 batches of samples we prepared. A total of 96 samples were examined to evaluate the variation of microstructure and mechanical properties. In fact, a mixed microstructure of α/β and martensite plates, a fine α/β dual phase microstructure and gradually coarsen α/β dual phase microstructure could be achieved [17]. As an example, Fig. 5 shows the change of microstructure with variation in speed function.

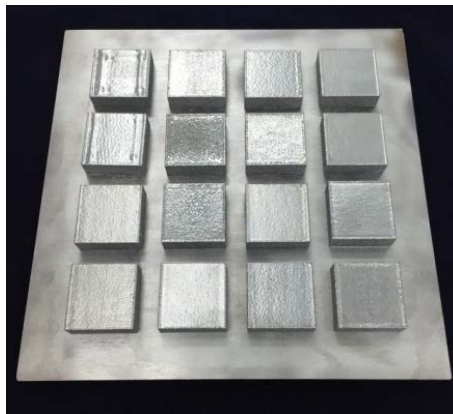


Fig. 4 Picture of samples (30×30×10 mm) prepared by Arcam EBM machine to evaluate the effect of processing parameters on microstructure and mechanical properties.

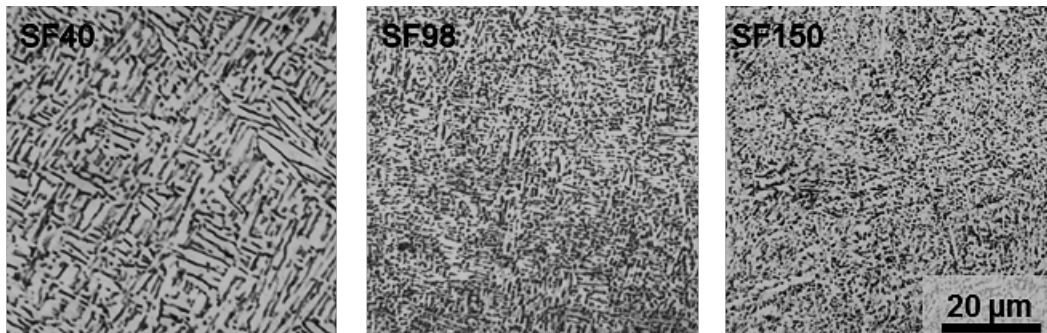


Fig. 5 Microstructure dependence of speed function (SF) in EBM-built parts.

By conducting post heat treatment, the as-built microstructure and mechanical properties can be modified. Because of thermal gradient along the build direction, the long columnar prior β grains is always observed in EBM-built Ti-6Al-4V [4, 11, 18], which causes an anisotropic mechanical properties [11]. Therefore, a wide range of heat treatment experiments were performed. Interesting relationship between the heat treatment cycles and their resultant

microstructure and the mechanical properties were observed. By modifying the morphology of the EBM-built microstructure, improved mechanical properties with equiaxed grains could be obtained via post heat treatment [19].

Besides, we also tried to control the texture in EBM Ti-6Al-4V by considering the solidification map for Ti-6Al-4V where the solidification rates (R) and thermal gradients (G) were extracted from numerical calculations [20]. Several calculations were carried out at different process parameters (for example scan speed and beam power) and the influence of the parameters on the texture can be observed by extracting G and R from the mushy zone and finding where the data falls on the solidification map in respect to the mixed-to-columnar and mixed-to-equiaxed boundaries. Unpublished numerical work done by the present authors indeed revealed that texture control in powder-bed fusion (PBF) of Ti-6Al-4V may be more challenging than for Ni-based superalloys [21, 22].

Porosity

Two types of pores (typical spherical pores and the irregular pores) can be observed in the EBM-built parts (Fig. 6). The irregular pores with large dimensions were caused by improper setting of processing parameters [17]. Small spherical pores that was a common phenomenon in AM Ti-6Al-4V parts [23-25] were observed and all the porosities were less than 0.25 vol. % in EBM-built parts [26]. The origin of small spherical pores is possibly related to the entrapped argon gas during the fabrication of gas atomized Ti-6Al-4V powder. Nevertheless, limited small pores with homogenous distribution in the built part will not adversely affect the microhardness and tension/compression mechanical properties of the EBM-built parts [24]. However, these existed pores degraded the fatigue properties of AM Ti-6Al-4V parts and are detrimental to components with fatigue application needs. Therefore, one of the efforts of the present authors is to improve the fatigue properties by minimizing the pore size and pore volume fraction via the optimization of the processing parameters [17] rather than via post processing, such as hot isostatic pressing that is a conventional method to improve fatigue properties of AM parts.

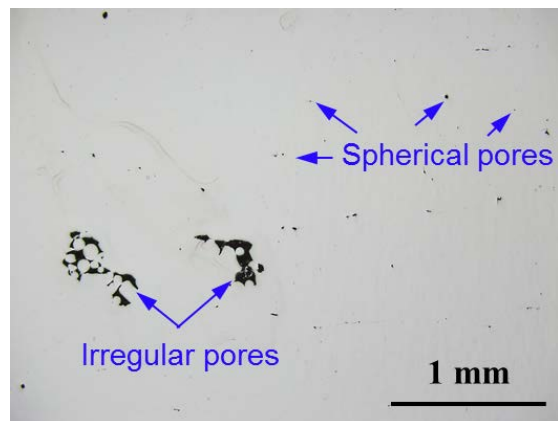


Fig. 6 Morphology of pores observed in EBM-built parts.

Surface finishing

Although the mechanical properties of machined EBM-built parts are comparable with that of the wrought counterparts [10, 11, 14, 15], the surface finishing of EBM-built parts is quite rough [4]. Fig. 7 shows the surface roughness measured from four big plates (Fig. 1c). It was revealed that the surface roughness was independent of build height, though the graded microstructure and mechanical properties were observed along the build height [15]. The rough surface is caused by the powder size which is in the range of 45-105 μm and the beam size which is $\sim 200 \mu\text{m}$ for the present Arcam A2X or A2XX machines. Unpublished results show that optimizing processing parameters and/or adopting fine powder are the possibilities to achieve a better surface roughness. In addition, we can orientate the critical surface of parts to specific positions to achieve better surface roughness. Fig. 8 shows the surface perturbations using optical profiler in the EBM-built specimen. Obviously, the top surface (Fig. 8a) has a better surface finish than the side surface (Fig. 8b).

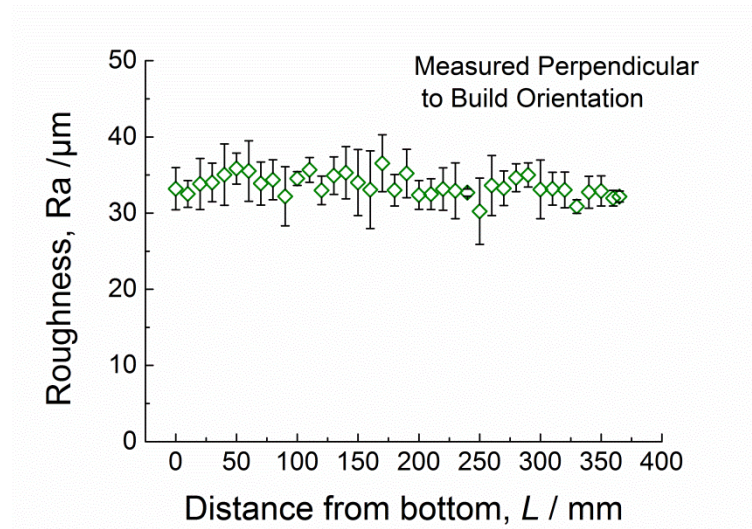


Fig. 7 Surface roughness dependence of build height in EBM-built Ti-6Al-4V.

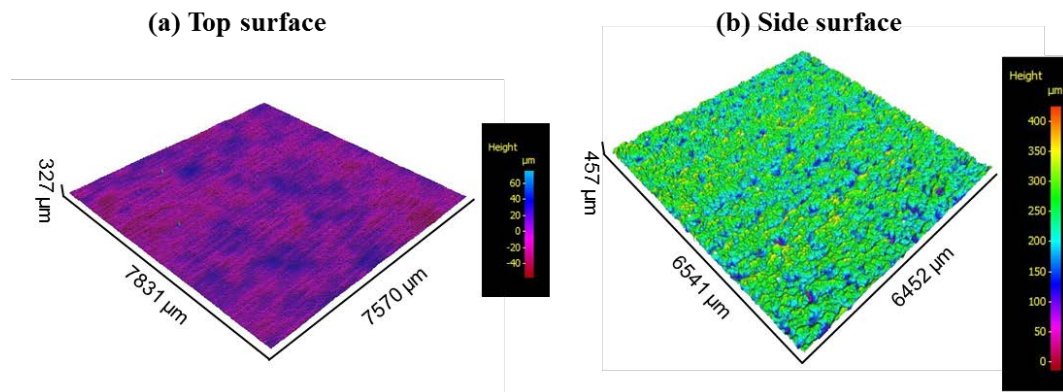


Fig. 8. Surface perturbations using optical profiler in the EBM-built specimen (a) top surface and (b) side surface.

Fig. 9 shows the pictures of EBM-built medium volume industrial parts. The dimensions of nozzle (Fig. 9a) and blade (Fig. 9b) are $\Phi 180 \times 300$ mm and $180 \times 70 \times 360$ mm, respectively. A visible rough surface is observed for the side surfaces rather than top surface (Fig. 9b). Moreover, a series of post treatments, such as (i) adaptive computer numeric control abrasive material removal process and (ii) chemical and plasma material removal process, is necessary if a better surface finish is required. A post treated blade that exhibits better surface finishing is shown in Fig. 9 (c).

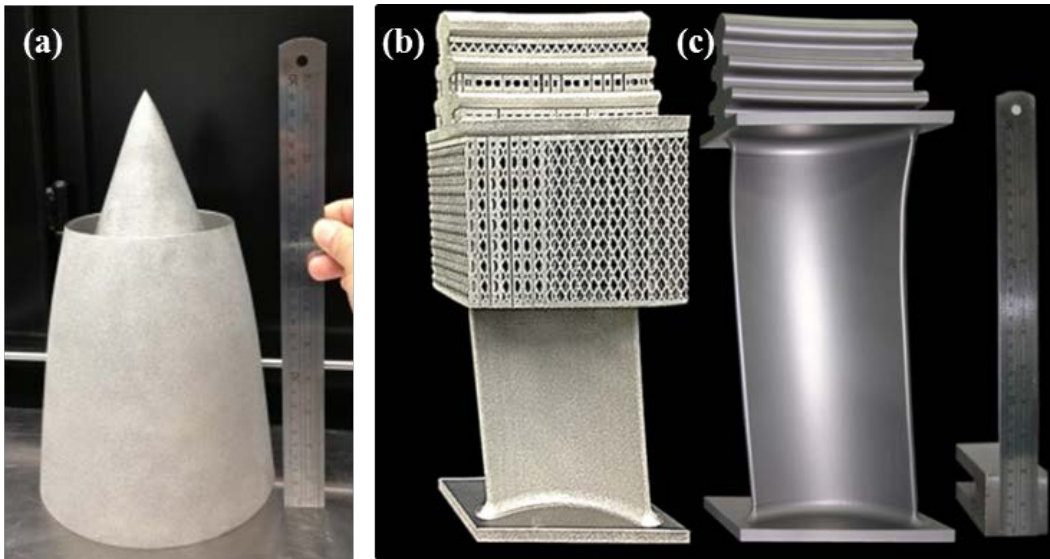


Fig. 9 Pictures of (a) EBM-built nozzle, (b) EBM-built blade and (c) polished blade.

Simulations of residual stress formation

It is believed that the EBM-built parts have a very low residual stress because of the elevated building temperature that acts as a stress relief heat treatment. However, it is important to obtain the exact value of residual stress in EBM-built parts and to further minimize the residual stress. Therefore, we numerically studied the formation of residual stress formation caused by the EBM process. This was motivated by the difficulty to obtain reliable measures of residual stress because of the rough surface of EBM-built parts. Our interest has been in understanding the quantitative role of process parameters such as beam size, scan speed, beam energy density and bed preheating temperature. Systematic calculations [25] showed that changing the beam parameters may not be the best strategy to minimize residual stress. In fact, the traditional metallurgy argument of processing at higher temperature had superior quantitative impact than the fine-tuning of the beam parameters. Our study revealed that the residual stress (Von Mises stress) in EBM-built parts is lower than 200 MPa, and decreased with increasing powder bed preheating temperature (Fig. 10) [25]. Even though high-temperature processing certainly requires adjustments in the melt theme parameters, the simulations suggest a route to avoid any post-processing stress-relief steps for

parts where a milder microstructure is acceptable and in conditions where smoke events and balling are kept under control.

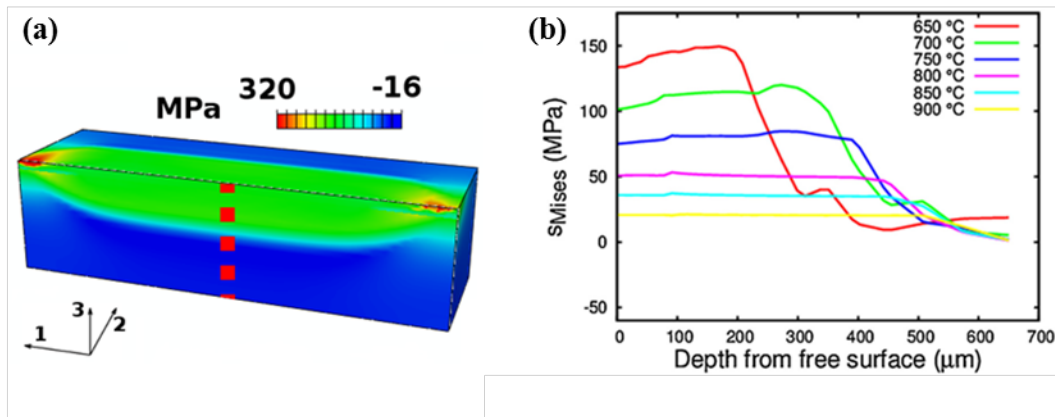


Fig. 10 Simulations of residual stress formation during single-track EBM scans. (a) Overall features of residual stress in cross-section and (b) line profiles along the red dashed line in (a) for different bed preheating temperatures.

Simulations of microstructure evolution

Simulations of PBF metal AM can complement experiments in a number of ways, including the understanding of the part's texture and microstructure. As discussed in the previous sections, both the texture and the microstructure of EBM parts are different from their cast or wrought counterparts. Specifically, the texture is different where columnar grains are dominant over equiaxed grains, while martensite or fine α dominates over the classical bimodal distribution. In reality, casting and metalworking equally result in textures and microstructures, which are not necessarily equiaxed and homogeneous. However, the anisotropies in AM parts are clearly larger. As pointed by Babu and coworkers [27], neither an isotropic, bimodal microstructure nor a directional, martensitic microstructure are necessarily "optimal" *per se*; rather, it is the purpose and design of the part that dictates its optimal texture and microstructure. In this regard, modeling and simulations can provide a fast and cost-effective tool to explore the parameters' processing window that affects the microstructure.

One of our interests is to understand why martensite could form in EBM. In our model, the volume fraction of martensite ($f_{\alpha'}$) was a new variable at each integration point, together with the fractions of α (f_{α}) and of β (f_{β}), such that $f_{\alpha} + f_{\beta} + f_{\alpha'} = 1$. At the same time, fortunately, this calculation is not problematic from a numerical standpoint because, as a solid-state transformation occurring below the β transus, the cooling rates are already significantly smaller than those during solidification. Specifically, at each integration point within the FEM mesh, the following conditions were checked: (i) temperature below the martensite start temperature (800 °C) and (ii) cooling rate faster than 410 °C/s [28]. If these conditions were met, the amount of available β was transformed into martensite. At the same time, the semi-empirical equation for martensite dissolution shown by Gil-Mul et al. [29] was

implemented. As a result, if an integration point had a non-null martensite volume fraction and the local temperature was sufficiently high, martensite could decompose. Here, the amount of decomposed martensite was equally redistributed into f_α and f_β at the following iteration step. After that, the equations for the evolution of α and β would update f_α and f_β to their new appropriate values. In summary, an example of such implementation is shown in Fig. 11, where simulations were performed to understand the effect of the different build temperatures between EBM and SLM and to correlate that with the different amounts of martensite typically seen in EBM and SLM samples [30].

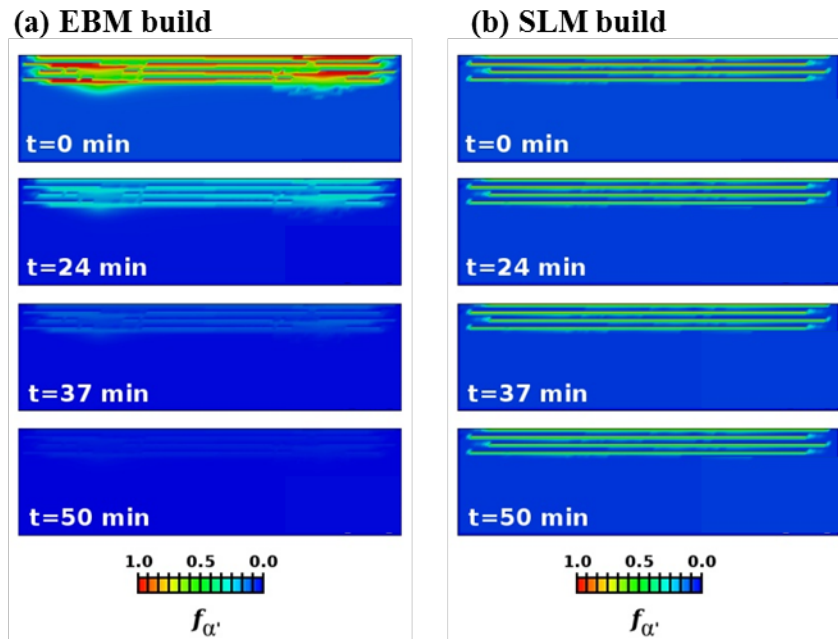


Fig. 11. Volume fraction of martensite during 4-layer (a) EBM build and (b) SLM build. Aside from small differences in the beam geometry which account for electron or laser beam, the main difference was the building temperature of (a) 650°C and (b) 30°C.

Conclusions

Overall, our work demonstrated that EBM processing resulted in a different microstructure and mechanical properties from other powder-based metal additive manufacturing technologies. The comprehensive understanding of microstructure evolution, mechanical properties variation, and residual stress distribution in EBM processing of Ti-6Al-4V is useful for the development of new materials in the future. The porosity and surface roughness on EBM-built component should be considered when EBM is applied to produce high performance components. Future work should be focused on understanding the pore formation mechanism and understanding the effect of surface roughness on the mechanical properties, such as tension/compression mechanical properties and cyclic deformation.

Acknowledgments

The authors are grateful for the financial support provided by A*STAR Industrial Additive Manufacturing Program: Work Package 3 (Electron Beam Melting), grant no. 132 550 4103.

References

- [1] S. Biamino^a, A. Penna^a, U. Ackelid^b, S. Sabbadinic, O. Tassad, P. Finoa, et al., Electron beam melting of Ti–48Al–2Cr–2Nb alloy: Microstructure and mechanical properties investigation, *Intermetallics* 19 (2011) 776-781.
- [2] O.L. Rodrigueza, P.G. Allisona, W.R. Whittington^b, D.K. Francis^b, O.G. Riveraa, K. Choua, et al., Dynamic tensile behavior of electron beam additive manufactured Ti6Al4V, *Mater. Sci. Eng., A* 641 (2015) 323–327.
- [3] S. Tammas-Williams, H. Zhao, F. Léonarda, F. Dergutib, I. Toddb, P.B. Prangnella, XCT analysis of the influence of melt strategies on defect population in Ti–6Al–4V components manufactured by Selective Electron Beam Melting, *Mater. Charact.* 102 (2015) 47-61.
- [4] P. Wang, X. Tan, M.L.S. Nai, S.B. Tor, J. Wei, Spatial and geometrical-based characterization of microstructure and microhardness for an electron beam melted Ti–6Al–4V component, *Mater. Des.* 95 (2016) 287-295.
- [5] P. Wang, Y. Feng, F. Liu, L. Wu, S. Guan, Microstructure and mechanical properties of Ti–Zr–Cr biomedical alloys, *Mater. Sci. Eng., C* 51 (2015) 148-152.
- [6] L. Li, D. Liu, Y. Chen, C. Wang, F. Li, Electron microscopy study of reaction layers between single-crystal WC particle and Ti–6Al–4V after laser melt injection, *Acta Mater.* 57 (2009) 3606-3614.
- [7] S.H. Mok, G. Bi, J. Folkes, I. Pashby, J. Segal, Deposition of Ti-6Al-4V using a high power diode laser and wire, Part II: Investigation on the mechanical properties, *Surf. Coat. Technol.* 202 (2008) 4613-4619.
- [8] L.E. Murr, S.A. Quinones, S.M. Gaytan, M.I. Lopez, A. Rodela, E.Y. Martinez, et al., Microstructure and mechanical behavior of Ti–6Al–4V produced by rapid-layer manufacturing, for biomedical applications, *J. Mech. Behav. Biomed. Mater.* 2 (2009) 20-32.
- [9] G. Reports. The FAA Cleared the First 3D Printed Part to Fly in a Commercial Jet Engine from GE.
<http://www.gereports.com/post/116402870270/the-faa-cleared-the-first-3d-printed-part-to-fly2015>.
- [10] L. Murr, E. Esquivel, S. Quinones, S. Gaytan, M. Lopez, E. Martinez, et al., Microstructures and mechanical properties of electron beam-rapid manufactured Ti–6Al–4V biomedical prototypes compared to wrought Ti–6Al–4V, *Mater. Charact.* 60 (2009) 96-105.
- [11] P. Wang, M.L.S. Nai, X. Tan, W.J. Sin, S.B. Tor, J. Wei, ANISOTROPIC MECHANICAL PROPERTIES IN A BIG-SIZED Ti-6Al-4V PLATE FABRICATED BY ELECTRON BEAM MELTING, *TMS 2016 Supplemental Proceedings* (2016) 5-12.

-
- [12] X. Tan, Y. Kok, W.Q. Toh, Y.J. Tan, M. Descoins, D. Mangelinck, et al., Revealing martensitic transformation and α/β interface evolution in electron beam melting three-dimensional-printed Ti-6Al-4V, *Sci. Rep.* 6 (2016) 26039.
- [13] X. Tan, Y. Kok, Y.J. Tan, G. Vastola, Q.X. Pei, G. Zhang, et al., An experimental and simulation study on build thickness dependent microstructure for electron beam melted Ti-6Al-4V, *J. Alloys Compd.* 646 (2015) 303-309.
- [14] X. Tan, Y. Kok, Y.J. Tan, M. Descoins, D. Mangelinck, S.B. Tor, et al., Graded microstructure and mechanical properties of additive manufactured Ti-6Al-4V via electron beam melting, *Acta Mater.* 97 (2015) 1-16.
- [15] P. Wang, M.L.S. Nai, W.J. Sin, J. Wei, Effect of Building Height on Microstructure and Mechanical Properties of Big-Sized Ti-6Al-4V Plate Fabricated by Electron Beam Melting, *MATEC Web Conf.* 30 (2015) 02001.
- [16] N. Ikeo, T. Ishimoto, A. Serizawa, T. Nakano, Control of mechanical properties of three-dimensional Ti-6Al-4V products fabricated by electron beam melting with unidirectional elongated pores, *Metall. Mater. Trans. A* 45 (2014) 4293-4301.
- [17] P. Wang, M.L.S. Nai, B. Aw, L., J. Wei. Effect of processing parameters on microstructure and mechanical properties of Ti-6Al-4V made by selective electron beam melting additive manufacturing. 2016 Annual International Solid Freeform Fabrication Symposium (SFF Symp 2016). Austin, Texas, USA2016.
- [18] S. Al-Bermani, M. Blackmore, W. Zhang, I. Todd, The origin of microstructural diversity, texture, and mechanical properties in electron beam melted Ti-6Al-4V, *Metall. Mater. Trans. A* 41 (2010) 3422-3434.
- [19] R. Srinivasan, M.L.S. Nai, P. Wang, W.J. Sin, T. Li, J. Wei. DEPENDENCE of MICROSTRUCTURE and MECHANICAL PROPERTIES on HEAT TREAT CYCLES of ELECTRON BEAM MELTED Ti-6Al-4V 2016 Annual International Solid Freeform Fabrication Symposium (SFF Symp 2016). Austin, Texas, USA2016.
- [20] S. Bontha, N. Klingbeil. Thermal process maps for controlling microstructure in laser-based solid freeform fabrication. *Solid freeform fabrication proceedings: Proc. 2003 Solid Freeform Fabrication Symposium*, Austin; 2003. p. 219-226.
- [21] R.R. Dehoff, M.M. Kirka, F. List, K.A. Unocic, W.J. Sames, Crystallographic texture engineering through novel melt strategies via electron beam melting: Inconel 718, *Mater. Sci. Technol.* 31 (2015) 939-944.
- [22] C. Körner, H. Helmer, A. Bauereiß, R.F. Singer. Tailoring the grain structure of IN718 during selective electron beam melting. *MATEC Web Conf.*; 2014. p. 08001.
- [23] S. Tammas-Williams, H. Zhao, F. Léonard, F. Derguti, I. Todd, P. Prangnell, XCT analysis of the influence of melt strategies on defect population in Ti-6Al-4V components manufactured by Selective Electron Beam Melting, *Mater. Charact.* 102 (2015) 47-61.
- [24] B.E. Carroll, T.A. Palmer, A.M. Beese, Anisotropic tensile behavior of Ti-6Al-4V components fabricated with directed energy deposition additive manufacturing, *Acta Mater.* 87 (2015) 309-320.
- [25] S.H. Mok, G. Bi, J. Folkes, I. Pashby, Deposition of Ti-6Al-4V using a high power diode laser and wire, Part I: Investigation on the process characteristics, *Surf. Coat. Technol.* 202 (2008) 3933-3939.

-
- [26] C. He, P. Wang, M.L.S. Nai, J. Wei. Distribution of porosity in electron beam melting additive manufactured Ti-6Al-4V component. In: T. Furuhashi MNaSM, editor. The Ninth Pacific Rim International Conference on Advanced Materials and Processing (PRICM9). Kyoto, Japan: The Japan Institute of Metals and Materials; 2016. p. 385-387.
- [27] W. Sames, F. List, S. Pannala, R. Dehoff, S. Babu, The metallurgy and processing science of metal additive manufacturing, *Int. Mater. Rev.* (2016) 1-46.
- [28] T. Ahmed, H.J. Rack, Phase transformations during cooling in $\alpha + \beta$ titanium alloys, *Mater. Sci. Eng., A* 243 (1998) 206-211.
- [29] F.G. Mur, D. Rodriguez, J. Planell, Influence of tempering temperature and time on the α' -Ti-6Al-4V martensite, *J. Alloys Compd.* 234 (1996) 287-289.
- [30] G. Vastola, G. Zhang, Q.X. Pei, Y.-W. Zhang, Modeling the Microstructure Evolution During Additive Manufacturing of Ti6Al4V: A Comparison Between Electron Beam Melting and Selective Laser Melting, *JOM* 68 (2016) 1370-1375.